# Interplay of Spin Conversion and Structural Phase Transformations

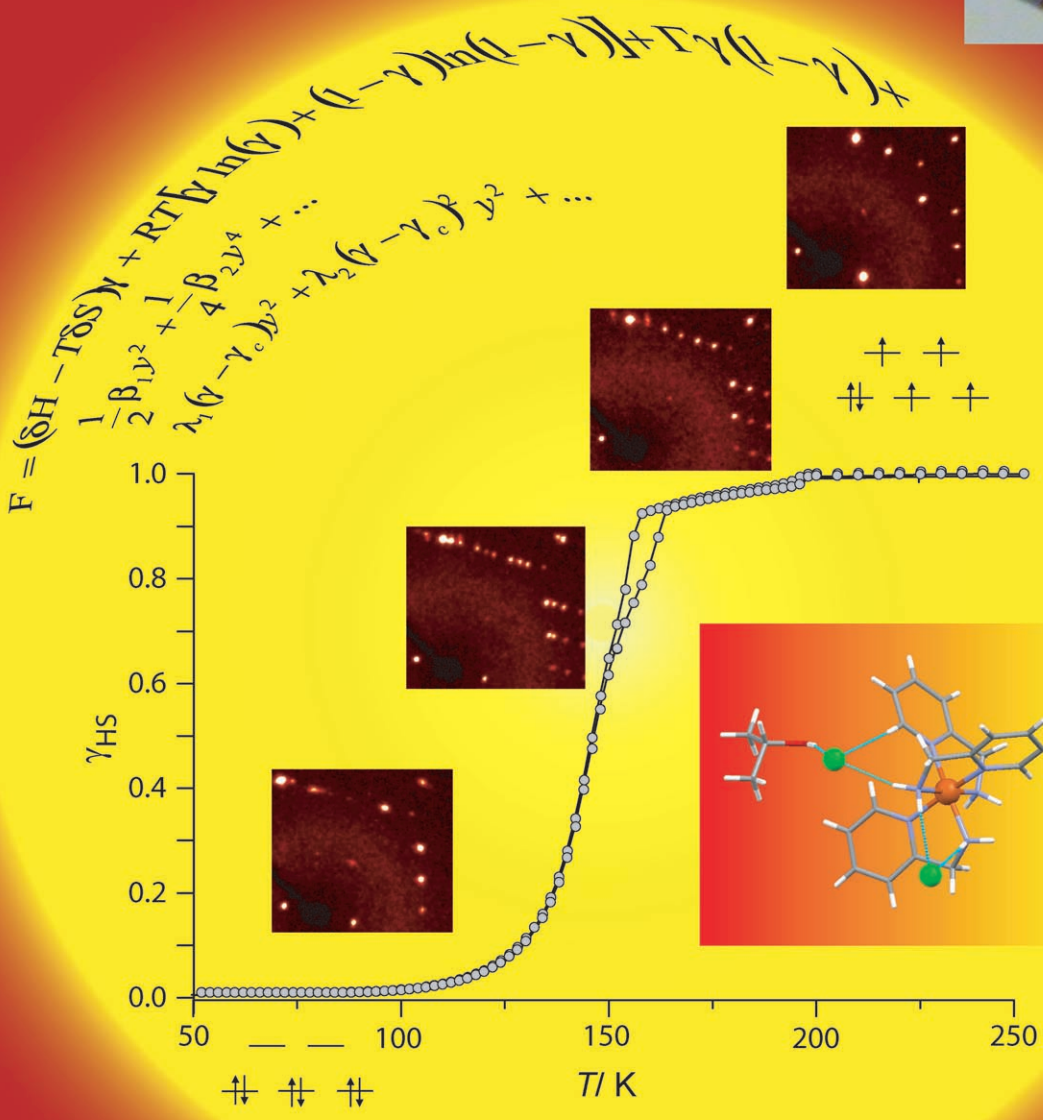


For more information see the following pages

CHEMISTRY
A EUROPEAN JOURNAL

DOI: 10.1002/chem.200600547

# Interplay of Spin Conversion and Structural Phase Transformations: Re-Entrant Phase Transitions in the 2-Propanol Solvate of Tris(2-picolylamine)iron(II) Dichloride

**Karl W. Törnroos,*[a] Marc Hostettler,[b] Dmitry Chernyshov,[c] Brita Vangdal,[a] and Hans-Beat Bürgi[b]**

**Abstract:** Crystal structures, magnetic and thermodynamic properties of the spin-crossover compound tris(2-picolylamine)iron(II) dichloride (with 2-propanol solvent molecules) have been measured in the temperature range from 15 to 293 K. X-ray diffraction, SQUID, and calorimetric experiments all showed two first-order phase transitions with hysteresis loops, a narrow one at $T_1 \sim 196$ K and a broad, triangular one covering the range $153 < T_2 < 166$ K. Crystal structures were analysed at fourteen temperatures in a cooling cycle and at seven temperatures in a heating cycle. They reveal a complex, temperature-dependent ordering behaviour of both the complex cations and the alcohol molecules. A phenomenological model accounting for spin conversion, solvent ordering and coupling between the two processes describes the observed phase transitions and ordering phenomena reasonably well. Similarities and differences in the behaviour of the corresponding ethanol solvate with the same crystal architecture are discussed. It is concluded that spin-crossover behaviour depends as much on molecular properties as it does on intermolecular interactions, both of the spin active and the spin inactive components.

**Keywords:** iron · phase transitions · solvent effects · spin crossover · X-ray diffraction

## Introduction

Much of the continuing activity in spin-crossover research on octahedral complexes with 3d metals is motivated by potential applications for display, memory and switching devices.[1–3] Such applications require materials that can be switched rather abruptly between states with different physical properties. There is still a debate whether such switching can be achieved with noninteracting, bistable molecules.[4] In the solid state molecular bistability is only one factor governing the changes of physical properties, another one being the interactions between the ions and molecules in a crystal. The complex interplay between molecular and crystal properties produces solid-state phenomena including not only bistability, but also multistability and complete suppression of changes in physical properties. This entire spectrum of behaviour has been observed serendipitously in a family of six chemically and structurally very closely related spin-crossover compounds, namely $[Fe^{II}(2\text{-pic})_3]Cl_2$ solvates with methanol, ethanol, 1-propanol, 2-propanol, *tert*-butanol and allyl-alcohol (2-pic: 2-picolylamine).[5] Our inability to correlate crystal structure parameters to the spin transition properties has motivated us to investigate these compounds in greater detail. Crystal structures and magnetic properties between liquid helium and room temperature of the ethanol solvate have been reported earlier;[6] corresponding information on the 2-propanol solvate is described in this work. The crystal structures of the two solvates are very similar; surprisingly their magnetic behaviour is quite different.

For octahedral iron(II) complexes like the $[Fe^{II}(2\text{-pic})_3]Cl_2$ solvates, the conversion is between the low-spin singlet state (LS, $S=0$, $(t_{2g})^6(e_g)^0$) and the high-spin quintet state (HS, $S=2$, $(t_{2g})^4(e_g)^2$). Quantum-chemical calculations on the isolated complexes seem to be a powerful tool to estimate the molecular contributions to the HS/LS enthalpy and entropy

[a] Prof. K. W. Törnroos, B. Vangdal
Department of Chemistry, University of Bergen
Allégt. 41, 5007 Bergen (Norway)
Fax: (+47) 55-589-490
E-mail: karl.tornroos@kj.uib.no

[b] Dr. M. Hostettler, Prof. H.-B. Bürgi
Laboratorium für Kristallographie, Universität Bern
Freiestr. 3, 3012 Bern (Switzerland)

[c] Dr. D. Chernyshov
SNBL at the ESRF, 6 rue Jules Horowitz
BP 220, 38043 Grenoble cedex 9 (France)

  

differences.[7,8] The molecular entropy increases on going from the LS to the HS state, due to the difference in spin multiplicity, to an increased flexibility of the HS state arising from the increase in metal–ligand bond lengths and to the appearance of disorder in the counterion and/or solvent molecules. Complicated and possibly cooperative interactions between the spin active cations, the anions and other molecules in the crystal structures also affect spin equilibria, but are much more difficult to understand.[9] If the spin changes are accompanied by order–disorder transitions involving any of the entities in the unit cell, configurational entropy is another factor to be taken into account. Thermally induced phase changes of spin-crossover compounds are expected to be accompanied by changes of physical properties including colour, magnetisation and molecular volume.

The dependence of spin conversion on external stimuli such as temperature and pressure is conventionally depicted with the help of so-called transition curves, which represent the evolution of the magnetic moment or of structural parameters during the transition from a HS phase at high temperatures to a mixed phase of HS and LS molecules at intermediate temperatures and eventually to a LS phase at low temperatures. Transition curves may be gradual or abrupt, show hysteresis, and be one- or multistep, thus suggesting scenarios ranging from gradual crossover to first-order, multistep transitions. In the case of gradual, one-step crossover the space groups of the HS and LS end members are the same, thus implying an isostructural scenario of spin transition;[9] at intermediate stages of the transition HS and LS molecules are disordered and show short-range order at best. In the case of a first-order transition, the crystal structures may retain or change crystal symmetry and separate HS and LS domains may coexist. Alternative scenarios characterised by two gradual or abrupt steps with a plateau near equal concentrations of HS and LS molecules have also been observed in a number of spin-crossover compounds.[6,10–12] In all two-step cases we are aware of, the crystal structures associated with a plateau in the spin transition curve differ from the HS and LS structures by having superstructure Bragg reflections, indicating a transition scenario with symmetry breaking. If the HS and LS phases in a two-step spin crossover are isostructural, the sequence of transitions is called "re-entrant". So far ordering of HS and LS molecules has been observed mostly near a HS concentration of ~50%. The models describing the different scenarios of spin transitions are usually based on an Ising-like phenomenological approach[13] or on a Landau expansion of the free energy.[9]

In this contribution we report on magnetic and calorimetric measurements as well as on a multitemperature single-crystal diffraction study of the $[Fe^{II}(2\text{-pic})_3]Cl_2\cdot$2-propanol solvate (**1**).[5] The crystal structure was measured at 21 temperatures, 14 of them covering a cooling cycle from 293 to 15 K, and 7 a heating cycle between 149 and 206 K. The transition curve based on magnetic data is thus endorsed by a microscopic characterisation of the thermal evolution of the crystal structure. Aspects of the spin-crossover behaviour of **1** deserving detailed discussion include:

1) The intermediate plateau occurs at an unusual HS concentration of ~95% and extends over a large temperature range, from ~200 to ~153 K; the corresponding crystal structure shows a doubled unit cell and the sequence of phases is re-entrant, analogous to, but different from that observed for other representatives of the family.
2) There is a remarkable correlation between spin populations of the iron complexes and the degree of ordering of the 2-propanol solvate molecules.
3) Diffraction experiments show coexistence of the ordered and intermediate phases which is paralleled by hysteresis in the spin transition curve.
4) A simple phenomenological model based on ideas of Drickamer and Slichter and of Landau, first suggested in reference [9], reproduces the observed transition scenario over a large temperature range.

## Results

**Magnetisation and differential scanning calorimetry (DSC)**: The transition curve of **1** shows an abrupt transition at $T_1$~196 K from a high-temperature phase which is 100% HS, to one which is ~98% HS (Figure 1, top); we call it the "HS intermediate phase" (HS IP). The transition shows a narrow hysteresis loop, no more than 1–2 K wide and is therefore first-order. Further decrease of temperature is accompanied by a slow decrease of the HS concentration until at $T$~158 K the HS fraction drops steeply. Below $T_{1/2}$~147 K the HS concentration decreases more gradually towards the LS state with complete conversion below ~100 K ($T_{1/2}$ is the temperature at which the concentrations of the HS and LS states are equal). Upon re-heating a hysteresis loop with an unusual triangular shape unfolds. It extends between $T$~153 and ~166 K and indicates another first-order phase transition occurring in this temperature range. On further heating the compounds reverts to its HS phase at $T_1$~196. Cooling the sample from room temperature to some temperature between 166 and 147 K and subsequent heating revealed inner hysteresis loops (Figure 1, top, insert). The DSC measurements confirm the first-order character of both transitions, the one from the high-temperature, pure HS phase to the HS IP, and from the HS IP to the LS/HS zone of the low-temperature phase (Figure 1, bottom). The hysteresis widths from DSC and SQUID measurements differ somewhat; we attribute this effect to the low heat conductivity of the sample, which could delay the appearance of a DSC signal at the heating and cooling rate used (10 K min$^{-1}$).[14] The broad bump found below the signals associated with the first-order transformation and centred at $T_{1/2}$ is a typical feature of a gradual spin crossover.[15]

Based on these observations the transition curve may be subdivided into the following, partly overlapping zones:

  

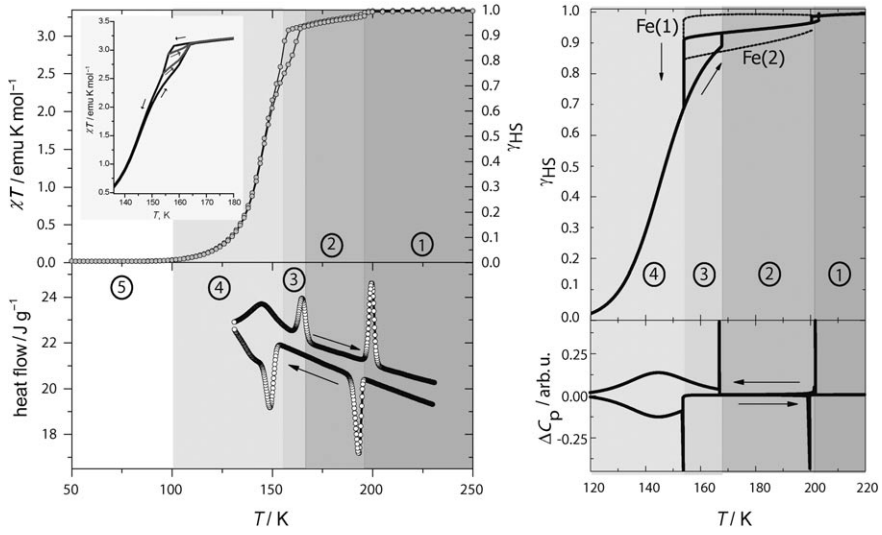


Figure 1. Macroscopic properties of $[Fe^{II}(2\text{-pic})_3]Cl_2 \cdot 2$-propanol (**1**) as a function of temperature. The numbered grey zones indicate the following macroscopic regimes (see text): 1) High-temperature phase, purely HS. 2) Intermediate HS phase (HS IP). 3) Hysteresis zone. 4) Low-temperature phase, HS/LS zone. 5) Low-temperature phase, purely LS. Top left: $\chi T$ from SQUID measurements, the insert shows inner hysteresis loops. Bottom left: heat flow as recorded by DSC for a heating and a cooling cycle. Top right: $\gamma(T)$ from a phenomenological model (see text). The temperature dependence of the average HS fraction is shown as a bold solid line, the HS fractions of the two different iron sites within zones 2 and 3 as thin dashed lines. Bottom right: specific heat from the phenomenological model (see text).

1) A high-temperature phase, purely HS, above ~196 K.
2) An intermediate HS phase (HS IP) bracketed between two first-order transitions, both associated with hysteresis loops, a narrow one at $T_1 \sim 196$ K and a broad one covering the range $153 < T_2 < 166$ K.
3) A triangular hysteresis zone between ~153 and ~166 K.
4) The HS/LS zone of a low-temperature phase with a HS fraction gradually decreasing from ~50 to 0% between 147 and ~100 K.
5) Continuation of the low-temperature phase below ~100 K, purely LS.

These five zones, defined on the basis of macroscopic properties, will now be further characterised in terms of the underlying crystal structures.

**Structural aspects**: The crystal structure of the high-temperature, pure HS phase of **1** has been reported before.[5] It is built from layers made of $Fe^{II}$ complexes hydrogen bonded through chlorine counterions, which also act as hydrogen-bond acceptors for the hydroxyl groups of the 2-propanol molecules. The hydroxyl groups are disordered over two sites. The 2-propyl groups, protruding out of a given layer, fit into the wedge-shaped cavities formed by pairs of pyridine rings belonging to an iron complex in the neighbouring layers. These and numerous other van der Waals contacts keep neighbouring layers together. The space group symmetry is $B2_1/c$; the asymmetric unit of the crystal structure is composed of one pair of chloride ions, one 2-propanol molecule and a single iron complex occupied with HS iron atoms (a nonconventional description has been chosen for ease of comparison with the other phases of **1** and with the crystal structures of the other members of the family; the transformation matrix from the standard description in space group $P2_1/a$ to $B2_1/c$ is [001] [010] [−20−1]).

During the first-order transition from the high-temperature phase to the HS IP at 196 K the crystal structure looses the B-centring and changes the space group to $P2_1/a$. The general architecture of the HS IP remains the same as that of the high-temperature phase, but its asymmetric unit now comprises two crystallographically inequivalent iron complexes, four chlorine ions, and two solvent molecules. HS complexes, hardly distinguishable from those in the pure HS phase, occupy one of the two iron sites. The other is occupied by a disordered mixture of HS and LS complexes, the composition of which changes from ~9:1 to ~8:1 with decreasing temperature. The ordered site with only HS iron complexes is associated through its chlorine ions with disordered 2-propanol molecules, while the disordered complex is associated with ordered solvent molecules. Within the layers the two sites are arranged in two different kinds of parallel zigzag chains alternating along the *b* axis (Figure 2, left).

Below 153 K the original translational symmetry with space group $B2_1/c$ is recovered and maintained down to 15 K. The asymmetric unit is reduced back to one iron complex, two chlorine ions, and one ordered solvent molecule. In the HS/LS zone of this low-temperature phase the HS and LS complexes are distributed in a largely uncorrelated manner as deduced from the absence of any noticeable diffuse scattering.

The following, additional observations are also worth noting: 1) the change of the average Fe–N bond length accompanying the changes in temperature and crystal phase correlates well with the spin transition curve derived from the magnetic data (Figure 1 and Figure 3); 2) the two first-order phase transitions are associated with strong elastic strain, as seen from the changes of the unit cell volume and of the monoclinic angle, the latter changing by nearly 10 degrees between 200 and 147 K (Figure 3); and 3) within the wide hysteresis region a superposition of the diffraction patterns of the HS IP and of the low temperature $B2_1/c$ phase is observed as illustrated by the zone images shown in Figure 4. Given the co-existence of two phases with such

  

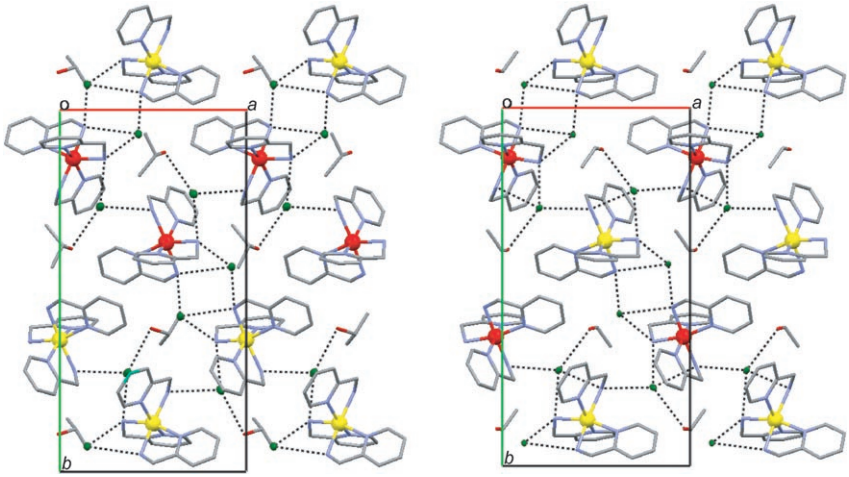


Figure 2. Packing diagrams of $[Fe(2\text{-pic})_3]Cl_2 \cdot 2$-propanol (**1**, left) and of the corresponding ethanol solvate (right) in their intermediate phases. Note the different ordering patterns indicated by red (LS) and yellow (HS) iron atoms. Chlorine atoms are shown as small green balls, hydrogen bonding is indicated by dashed, black lines.

dramatic differences in unit cell shape, it seems remarkable that some samples survived the changes in temperature and in some instances still produce single-crystal diffraction images after having shown phase coexistence.

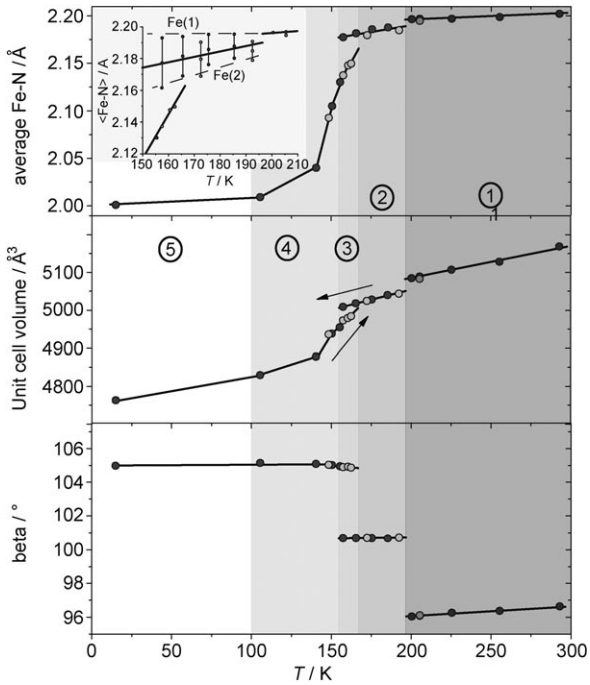


Figure 3. Structural properties of $[Fe(2\text{-pic})_3]Cl_2 \cdot 2$-propanol (**1**) as a function of temperature. Top: average iron–nitrogen bond lengths; the insert shows the overall average bond lengths and the separate averages for the two crystallographically inequivalent iron complexes in the HS IP region. Middle: unit cell volume. Bottom: monoclinic angle undergoing two jumps at the first order transformations. Dark-grey balls represent measurements from a cooling cycle, light-grey balls from a heating cycle. Solid lines are guides for the eye. The numbered grey zones have the same meaning as in Figure 1.

**Modelling the transition curve**: The macroscopic and diffraction experiments have uncovered a re-entrant sequence of two first-order phase transitions with hysteresis. Whereas the spin transition curve of the ethanol solvate is nearly symmetric with respect to $T_{1/2}$,[6] the corresponding curve of **1** is highly asymmetric. To account for this particular combination of spin conversion and phase transformations, we found it useful to somewhat modify [Eq. (1)] the classical Landau expansion of the free energy of a spin transition[9] as justified in the discussion part below:

$$F = (\Delta H - T\Delta S)\gamma + RT[\gamma \ln(\gamma) + (1-\gamma)\ln(1-\gamma)] + \Gamma\gamma(1-\gamma) + \frac{1}{2}\beta_1\gamma^2 + \frac{1}{4}\beta_2\gamma^4 + \ldots \lambda_1(\gamma-\gamma_c)\gamma^2 + \lambda_2(\gamma-\gamma_c)^2\gamma^2 + \ldots \quad (1)$$

The first line represents the free energy of spin crossover in the Slichter–Drickamer representation.[16] It is closely similar to the mean-field Gorsky–Bragg–Williams expression[17] and related to the conventional Ising-like model for a spin-crossover system.[18] In this expression $\Delta H$ and $\Delta S$ are the enthalpy and entropy changes associated with the spin conversion of the complex; they include both molecular and solid-state packing contributions. The term in $RT$ is the configurational (mixing) entropy; $\Gamma$ is a phenomenological "cooperativity parameter" for the spin-conversion process. The quantity $\gamma$ denotes the fraction of HS states, $\gamma = N_{HS}/N$, in which $N_{HS}$ is the number of iron complexes in the HS state and $N$ is the total number of spin active complexes. In the high-temperature phase of **1** $\gamma \sim 1$, in the low-temperature phase $\gamma < 0.5$, with $\gamma = 0$ at 15 K corresponding to the LS end member. The scalar quantity $\gamma$ is thus taken as the order parameter (OP) for the spin transition, which is not symmetry breaking. The second line in Equation (1) gives the Landau expansion of the excess free energy associated with the ordering process. The third line introduces the coupling between spin conversion and ordering. The coefficients $\beta_i$ and $\lambda_i$ are phenomenological constants. The coefficient $\beta_1$ is assumed to be a linear function of temperature, $\beta_1 = b(T-T_c)$; it is negative below $T_c$, the temperature close to which the phase transition may take place; $\beta_2$ is $>0$ to assure stability of the intermediate phase. The quantity $\gamma_c$ is the fraction of HS states in the vicinity of which the phase transition takes place. The OP $y$ characterises the degree of ordering in the sites of the HS IP, which are occupied by HS

  

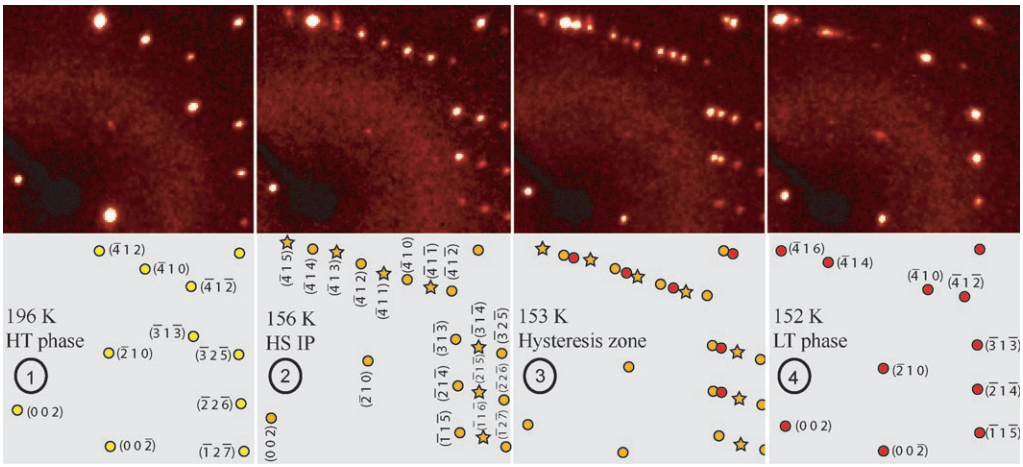


Figure 4. Upper panels: ($h0l$) zone images of **1** at 196, 156, 153 and 152 K. Lower panels: schematic interpretation of the diffraction images. The circled numbers have the same meaning as in Figure 1. (Codes: Circles: reflections with $h+l=2n$; stars: reflections with $h+l=2n+1$; light yellow: high-temperature phase; dark yellow: HS IP; red: low-temperature phase, HS/LS zone). In the hysteresis zone 3 the diffraction patterns of both the HS IP (dark yellow) and the low-temperature phase (red) appear.

and LS complexes or by orientationally disordered solvent molecules. For a model with equal numbers of nodes in both sublattices and in the neighbourhood of $\gamma_c=1/2$, $y$ is conveniently chosen as $2(N^A_{HS}-N^B_{HS})/N=\gamma^A-\gamma^B$, in which $N^A_{HS}(N^B_{HS})$ denotes the number of iron complexes in the HS state in sublattice $A(B)$, also $0\le\gamma^B\le\gamma^A\le1$ in analogy to $0\le\gamma\le1$ for one sublattice. For $\gamma_c\neq0.5$ this definition of $y$ is suitably normalised [Eq. (2)]:

$$y=\begin{cases}\dfrac{\gamma^A-\gamma^B}{2(1-\gamma)}, \gamma_c>1/2\\ \dfrac{\gamma^A-\gamma^B}{2\gamma}, \gamma_c<1/2\end{cases} \tag{2}$$

The physical meaning of $y$ is analogous to that for ordering of binary alloys. It always equals one if, for a given $\gamma$, the difference $|\gamma^A-\gamma^B|$ between the two sublattices is maximal. In the expansion in Equation (1) the terms in $y$ are all even, as required by the irreducible representation $Y_2^+$ associated with the observed change of symmetry during the phase transitions of **1**.[19] The coupling between the two processes includes linear-quadratic ($\propto y^2\gamma$) and bi-quadratic ($\propto y^2\gamma^2$) terms, both of which are symmetry allowed.

The temperature evolution of the system follows from the equilibrium conditions [Eq. (3)]:

$$\frac{\partial F}{\partial\gamma}=0=\Delta H-T\Delta S+RT\ln\left(\frac{\gamma}{1-\gamma}\right)+\Gamma(1-2\gamma)+\lambda_1y^2+2\lambda_2(\gamma-\gamma_c)y^2 \tag{3a}$$

$$\frac{\partial F}{\partial y}=0=[b(T-T_c)+\beta_2y^2+2\lambda_1(\gamma-\gamma_c)+2\lambda_2(\gamma-\gamma_c)^2]y \tag{3b}$$

The well-known temperature dependence of $\gamma$ describing normal spin crossover uninterrupted by a structural phase transition[18] follows from Equation (3a) with the trivial solution of Equation (3b), $y=0$ [Eq. (4)]:

$$T=\frac{\Delta H+\Gamma(1-2\gamma)}{\Delta S+R\ln\left(\frac{1-\gamma}{\gamma}\right)} \tag{4}$$

The intermediate phase (HS IP) is associated with the nontrivial solution of Equation (3b), $y^2\ge0$ [Eq. (5a)]:

$$y^2(T)=-\frac{1}{\beta_2}[b(T-T_c)+2\lambda_1(\gamma-\gamma_c)+2\lambda_2(\gamma-\gamma_c)^2] \tag{5a}$$

or in more compact form [Eq. (5b)]:

$$y^2(T)=-\frac{1}{\beta_2}(b(T-\tilde{T}_c)+2\lambda_2(\gamma-\tilde{\gamma}_c)^2)$$
$$\text{with } \tilde{T}_c=T_c+\frac{{\lambda_1}^2}{2b\lambda_2} \text{ and } \tilde{\gamma}_c=\gamma_c-\frac{\lambda_1}{2\lambda_2} \tag{5b}$$

The role of the linear quadratic term $\lambda_1(\gamma-\gamma_c)y^2$ in Equation (1) is therefore to renormalise critical concentration and temperature, as shown before for $\gamma_c\approx0.5$.[9] In the following we use renormalised parameters.

The domain of existence of the intermediate phase (HS IP, $y\neq0$) in terms of $\gamma$ values follows from Equations (4) and (5), specifically from the roots of the equation [Eq. (6)]:

$$-\frac{2\lambda_2}{b}(\gamma-\tilde{\gamma}_c)^2+\tilde{T}_c=\frac{\Delta H+\Gamma(1-2\gamma)}{\Delta S+R\ln\left(\frac{1-\gamma}{\gamma}\right)} \tag{6}$$

Within this domain the temperature dependence of the order parameter $\gamma$ can be found [Eq. (7)] from the equilibri-

  

um conditions [Eq. (3)]:

$$T = \frac{\Delta H + \Gamma(1-2\gamma) + 2\lambda_2(\gamma-\tilde{\gamma}_c)[b\tilde{T}_c - 2\lambda_2(\gamma-\tilde{\gamma}_c)^2]/\beta_2}{\Delta S + R\ln\left(\frac{1-\gamma}{\gamma}\right) + 2b\lambda_2(\gamma-\tilde{\gamma}_c)/\beta_2} \quad (7)$$

The temperature dependence of $y$ follows from Equation (5a). Outside the range of existence of the intermediate phase $y=0$ and the normal spin-crossover regime according to Equation (4) is recovered.

The changes in entropy and heat capacity associated with spin and structural transitions follow from the first and second derivatives of the total free energy [Eq. (1)] with respect to temperature. Abrupt changes of order parameters are associated with sharp peaks in the heat capacity and superimposed on a broad bump at $T_{1/2}$. A numerical illustration of the expected temperature dependences of the HS fraction $\gamma$ and the OP $y$ is shown in Figure 1 (right). The model parameters used in the numerical calculations are: $\Delta H = 4.41\ \mathrm{kcal\,mol^{-1}}$, $\Delta S = 0.03\ \mathrm{kcal\,mol^{-1}\,K^{-1}}$, $\Gamma = 0.1\ \mathrm{kcal\,mol^{-1}}$, $\tilde{\gamma}_c = 0.94$, $\tilde{T}_c = 605$ K, $b = 0.005$, $\beta_2 = 100$, $\lambda_2 = 500$. Comparison of the calculated and the experimental data shows that the model catches the essential features observed in the magnetic, calorimetric and diffraction experiments: a plateau in the transition curve at $\gamma \sim 0.95$, different HS populations in the two sublattices within the plateau, the first-order character of both phase transformations, a triangular hysteresis loop and sharp peaks in the heat capacity superimposed on a broad bump at $T_{1/2}$. There are several quantitative differences, however. The one in the temperature evolution of the HS concentrations on the two iron sublattices in the HS IP may be traced to the truncation of the Landau expansion for the ordering process and the coupling of the order parameters to fourth and second order terms in $y$, respectively; qualitative conclusions are not affected by the truncation. The difference in the slopes of the hysteresis walls, especially those in the cooling cycle, is probably related to phase coexistence and defect-related smearing of the transition, which is not included in the present model.

## Discussion

The 2-propanol solvate (**1**) and the ethanol analogue are chemically and structurally very similar and they both show two consecutive, re-entrant structural phase transitions.[6] There are important qualitative and quantitative differences, however.[5] In the ethanol solvate ordering occurs at ~50% HS concentration, whereas for **1** it happens near ~95%. In the former the HS and LS species within a hydrogen-bonded layer order—nearly completely—in a chessboardlike pattern, whereas in **1** they form an arrangement of alternating zigzag chains; the complexes in one chain are nearly all HS and those in the other present a disordered mixture of HS and LS states (Figure 2). The two compounds also differ in the temperature evolution of the solvent disorder.[5] All these differences are achieved by simply changing an ethyl group to a 2-propyl group in an otherwise unchanged crystal architecture. For example, average iron–ligand bond lengths are practically the same for both solvates in the HS phase at 200 K, 2.192(1) Å for the ethanol and 2.196(2) Å for the 2-propanol solvate. There are numerous changes of van der Waals contacts,[5] but their influence on the packing and the spin crossover behaviour is too complex to understand, let alone to predict.

In the LS phases differences in the average Fe–N distances between the two solvates appear more significant: 2.012(2) Å for the ethanol (12 K) and 2.000(2) Å for the 2-propanol solvate (15 K). The longer distance for the ethanol analogue indicates a somewhat weaker ligand field, in agreement with the fact that $T_{1/2}$ of the ethanol solvate is lower than $T_{1/2}$ of the 2-propanol solvate by ~20 K. However, such correlations have to be taken with a grain of salt, since the difference in bond length is marginal (0.012(3) Å). In addition there are factors other than the ligand field influencing the transition temperature; vibrational contributions and different degrees of disorder of the solvent molecules are but two of them.

Hysteresis behaviour marks another difference between the two solvates: no hysteresis has been found for the ethanol derivative, while a distinct triangular hysteresis loop is observed for **1** at the low-temperature side of the HS IP (Figure 1). Within this loop macroscopic domains of the HS IP and of the disordered LS/HS zone of the low-temperature phase coexist, a conclusion that follows from the simultaneous appearance of Bragg reflections from both phases at 153 K (Figure 4). Such phase coexistence has also been observed in other spin crossover solids at very low temperatures, when the light-induced HS phase relaxes towards the LS ground state.[10,20] A loop similar to that in **1** has been observed in the $[Fe^{II}(2\text{-pic})_3]Br_2$ ethanol solvate, but no structural interpretation has been given so far.[21]

For the ethanol solvate the free-energy change due to spin crossover was modelled with a minimal Landau potential including only first, second and fourth order terms.[9] This approximation holds best around $\gamma = 0.5$, that is, in the neighbourhood of the crossover and first-order phase-transition temperatures $T_{1/2}$, but does not show the required asymptotical behaviour of the transition curve: it exceeds the limiting values of $\gamma = 1$ and 0 at high and low temperatures, respectively. In the case of **1** the intermediate phase occurs close to $\gamma = 1$. It is therefore desirable to have a faithful description of the spin transition part of the model across the entire range $0 \le \gamma \le 1$. The Slichter–Drickamer expression for the free energy [Eq. (1), first line] does indeed show the correct asymptotic behaviour at high and low temperatures. The quantities in this expression are in the form of the enthalpy and entropy changes during spin crossover, the mixing entropy coming from the solid solution of the HS and LS complexes, and of a cooperativity parameter. Formally they appear to be quite different from the constants multiplying the polynomial terms in the order parameters of a Landau potential. However, in either case the re-

  

spective constants must be considered as phenomenological parameters chosen to reproduce experimental data.

For both the ethanol and 2-propanol solvates the ordering processes of the solvate molecules and the coupling between spin-related and spin-independent processes have been expressed with a Landau expansion, the minimal algebraic form of which has been found from symmetry arguments. The resulting model is capable to map a plateau in the transition curve centred at any critical HS concentration. By virtue of the coupling terms it also accounts for the different spin crossover behaviour of the two different sites in the HS IP of **1**. The rather drastic changes of the size and the shape of the unit cell with temperature (Figure 3) may be taken into account by bringing in a coupling between lattice strains and order parameters.[22]

The model given in Equation (1) may be generalised to spin transitions accompanied by any structural transformation. Note, however, that the phenomenological constants in the thermodynamic functions do not have an evident interpretation in terms of a specific microscopic model of a given substance, and thus no clear-cut microscopic significance. Nevertheless, our phenomenological approach uncovers the generic nature of multistability in spin-crossover solids, namely coupling between single-site spin crossover and degrees of freedom responsible for structural ordering.

Changes in solvent disorder not only contribute to changes in entropy during the spin-crossover process, but may also trigger the transition.[23,24] It was suggested that solvent disorder in the $[Fe^{II}(2\text{-pic})_3]Cl_2$ ethanol solvate modifies the elastic properties and therefore affects spin conversion.[25] We note that the role of the solvent molecules is more complex, at least in the series of $[Fe^{II}(2\text{-pic})_3]Cl_2$ solvates. The diffraction study of **1** shows that the OH···Cl and the NH···Cl hydrogen bonds may change by as much as 0.1 Å across the phase transitions. Similarly the orientation of the pyridine rings relative to the *ab* plane may change by up to 6°; assuming a radius of ~6 Å for the complex cation, such reorientations correspond to displacements of the peripheral hydrogen atoms again amounting to ~0.1 Å. These perturbations at or in the immediate environment of the $[Fe^{II}(2\text{-pic})_3]$ units are related to the cooperativity of spin crossover in a complicated way that does not seem to follow simple rules.[5] This problem is best illustrated by reiterating the fact that in the series of isostructural $[Fe^{II}(2\text{-pic})_3]Cl_2$ solvates we have observed not only bistability, tristability and a range of transition temperatures, but also cases of complete suppression of spin conversion. These results and especially the detailed findings described for the 2-propanol and ethanol solvates illustrate that cooperative transitions between two states in crystals built from bistable constituents are but the simplest among a multitude of possible scenarios, only some of which have been observed experimentally or predicted theoretically so far.

## Experimental Section

Compound **1** was synthesised and crystallised according to a published method.[26] The procedures for measuring and reducing the magnetisation data are described in reference [5]. Heat flow has been recorded using a differential scanning calorimeter (Perkin Elmer Pyris 1, DSC) with heating and cooling rates of 10 K min$^{-1}$.

Single-crystal diffraction data were collected in cooling and heating cycles. The former included measurements at 293, 256, 226, 206, 201, 186, 176, 166, 158, 156, 151, 141, 106 and 15 K, the latter at 149, 158, 161, 163, 173, 193 and 206 K. The data at 293 and 15 K data were collected at the Swiss–Norwegian beam lines at the ESRF (Grenoble, France) with focusing optics and $\lambda = 0.7100(1)$ Å. The 293 K data were recorded on a MAR345 image-plate detector using $\phi$-scans of 1.5° and a readout pixel resolution of 150 μm. The 15 K data were recorded with an Oxford Diffraction Onyx CCD detector using $\omega$ scans of 1° and an Oxford Diffraction HeliJet open-flow He-cryostat. Intensities were integrated with CrysAlis,[27] reflections shadowed by the cryostats were removed from the data by means of locally written software. The data for all other temperature points were collected with a Bruker AXS SMART 2 K CCD diffractometer by means of 0.3° $\omega$ scans with $Mo_{K\alpha}$ radiation ($\lambda = 0.71073$ Å) using SMART and were integrated using SAINT.[28] Samples were cooled with an Oxford Cryostream series 600 cryostat. Experiments above and within the hysteresis zone were achieved through gradual cooling. Due to the drastic changes in the monoclinic angle at the two transition points, acceptable crystal quality below the second transition point could only be achieved through flash cooling of the sample to a temperature below the transition point, that is, < 153 K. Crystals with an anisotropic shape, that is, flatter prisms (predominant faces in P setting, {1 0 0}), were less prone to cracking than more isotropic prisms. Mounting of crystals on to glass fibres was best done on one of the smaller faces, typically {0 2 1}. In total eight different crystal specimens were used to gather the 21 data sets. Of these six were taken within the triangular hysteresis loop, three on cooling and three on heating.

All data apart from the two synchrotron sets, were subject to numerical absorption correction using XPREP.[29] Empirical absorption correction was applied to the two latter sets using SADABS.[29] Structure solution and model refinement was done using SHELXS-97 and SHELXL97.[30]

CCDC-604575–604595 contains the supplementary crystallographic data for this paper. These data can be obtained free of charge from The Cambridge Crystallographic Data Centre via www.ccdc.cam.ac.uk/data_request/cif.

## Acknowledgements

This work was supported by the Norwegian Research Council and the Swiss National Science foundation. We thank the staff of the Swiss Norwegian Beam Lines (SNBL) at the European Synchrotron Research Facility for their support.

[1] P. Gütlich, Y. Garcia, H. Spiering in *Magnetism: Molecules to Materials IV* (Eds.: J. S. Miller, M. Drillon), Wiley-VCH, Weinheim, **2002**, pp. 271–344.
[2] O. Kahn, C. J. Martinez, *Science* **1998**, *279*, 44–48.
[3] A. Bousseksou, G. C. Molnar, *C. R. Chim.* **2003**, *6*, 1175–1183.
[4] H. Bolvin, O. Kahn, B. Vekhter, *New J. Chem.* **1991**, *15*, 889–895.
[5] M. Hostettler, K. W. Törnroos, D. Chernyshov, B. Vangdal, H.-B. Bürgi, *Angew. Chem.* **2004**, *116*, 4689–4695; *Angew. Chem. Int. Ed.* **2004**, *43*, 4589–4594.
[6] D. Chernyshov, M. Hostettler, K. W. Törnroos, H.-B. Bürgi, *Angew. Chem.* **2003**, *115*, 3955–3960; *Angew. Chem. Int. Ed.* **2003**, *42*, 3825–3830.
[7] M. Reiher, *Inorg. Chem.* **2002**, *41*, 6928–6935.

  

[8] H. Paulsen, A. X. Trautwein, *J. Phys. Chem. Solids* **2004**, *65*, 793–798.
[9] D. Chernyshov, H.-B. Bürgi, M. Hostettler, K. W. Törnroos, *Phys. Rev. B* **2004**, *70*, 094116.
[10] N. Huby, L. Guerin, E. Collet, L. Toupet, J.-C. Ameline, H. Cailleau, T. Roisnel, T. Tayagaki, K. Tanaka, *Phys. Rev. B* **2004**, *69*, 020101.
[11] D. Boinnard, A. Bousseksou, A. Dworkin, J. M. Savariault, F. Varret, J.-P. Tuchagues, *Inorg. Chem.* **1994**, *33*, 271–281.
[12] D. L. Reger, C. A. Little, V. G. Jr., Young, M. Pink, *Inorg. Chem.* **2001**, *40*, 2870–2874.
[13] R. Boča, W. Linert, *Monatsh. Chem.* **2003**, *134*, 199–216.
[14] R. Boča, M. Boča, H. Ehrenberg, H. Fuess, W. Linert, F. Renz, I. Svoboda, *Chem. Phys.* **2003**, *293*, 375–395.
[15] T. Nakamoto, Z.-C. Tan, M. Sorai, *Inorg. Chem.* **2001**, *40*, 3805–3809.
[16] C. P. Slichter, H. G. Drickamer, *J. Chem. Phys.* **1972**, *56*, 2142–2160.
[17] a) W. S. Gorsky, *Z. Phys.* **1928**, *50*, 64–88; b) W.L Bragg, E. J. Williams, *Proc. R. Soc. London Ser. A* **1934**, *145*, 699.
[18] H. Bolvin, *Chem. Phys.* **1996**, *211*, 101–114.
[19] H. T. Stokes, D. M. Hatch, *Isotropy Subgroups of the 230 Crystallographic Groups*, World Scientific, Singapore, **1988**.
[20] S. Pillet, J. Hubsch, C. Lecomte, *Eur. Phys. J. B* **2004**, *38*, 541–552.
[21] L. Wiehl, G. Kiel, C. P. Kohler, H. Spiering, P. Gütlich, *Inorg. Chem.* **1986**, *25*, 1565–1571.
[22] E. K. H. Salje, *Phase Transitions in Ferroelastic and Co-Elastic Crystals*, Cambridge University Press, **1990**.
[23] K. Kaji, M. Sorai, *Thermochim. Acta* **1985**, *88*, 185–190.
[24] M. Mikami, M. Konno, Y. Saito, *Chem. Phys. Lett.* **1979**, *63*, 566–569.
[25] T. Luty, K. Yonemitsu, *J. Phys. Soc. Jpn.* **2004**, *73*, 1237–1243.
[26] M. Sorai, J. Ensling, P. Gütlich, *Chem. Phys.* **1976**, *18*, 199–209.
[27] CrysAlis Software System, Ver. 1.169, Oxford-diffraction Ltd. Oxford (England), **2001**.
[28] SMART, Ver. 5.054 & SAINT, Ver. 6.45a, Bruker AXS Inc., Madison, Wisconsin (USA), **2001**.
[29] G. M. Sheldrick, SADABS, Ver. 2004/1 & XPREP Ver. 6.14, University of Göttingen, Göttingen (Germany), **2003**.
[30] G. M. Sheldrick, SHELXS-97 & SHELXL97, University of Göttingen, Göttingen (Germany), **1997**.

Received: April 17, 2006
Published online: July 14, 2006

  